Chapter 4

Tm on W(110): A Growth Study by Scanning Tunneling Microscopy

David Coffey, José I. Arnaudas, David Serrate and Miguel Ciria

Additional information is available at the end of the chapter

http://dx.doi.org/10.5772/intechopen.70218

Abstract

Exploring bottom-up procedures to achieve island and particles with a defined size can open opportunities in many applications. This contribution focuses on the growth of epitaxial Tm islands, below the monolayer range, on the W(110) surface by studying in situ the diffusion process at high temperature, between 700 and 1200 K, by means of scanning tunnel microscopy (STM) to determine the topography of the Tm deposits as a function of the coverage and thermal treatments of an initial room temperature deposit. Samples subject to a prolonged heating process, spending several hours at temperatures below 700 K, show that the average Tm islands size remains constant at higher temperatures, in contrast with samples subject to a faster heating. It is observed that the presence of carbon strongly limits the diffusion of Tm, thus leading to the formation of pseudomorphic nanometric islands instead of a full monolayer.

Keywords: surface diffusion, scanning tunneling microscopy, rare earth nanostructures, nucleation, self-organization

1. Introduction

Growing rare earth (RE) on the (110) surface of bcc metals (Mo, W, or Nb) has been widely used to obtain layers with the basal plane of the rare earth on this film plane [1–5]. Although the (110)bcc and (0001)hcp surfaces do not match with each other and therefore, the concept of epitaxial growth is not applicable; it has proven to still be possible to prepare quite perfect superlattices and films. Historically, the preparation of rare earth artificial superlattices dates from 1985 [1], with the Gd-Y system showing a novel magnetic behavior that has been

relevant in the history of nanostructured magnetic materials, as it was the first observation of antiferromagnetic coupling between ferromagnetic blocks occurring through a nonmagnetic spacer [4].

The (110) surface of W offers the opportunity of studying the magnetic behavior of ordered RE overlayers on top of a conductive but nonmagnetic substrate. In general, the body-centered cubic crystals of refractory metals such as W and Mo promote the two-dimensional layer growth of RE with no intermixing [6–8] with the (110) surface, yielding morphologies with low corrugation.

Thulium represents an interesting case, since it is the only heavy RE which orders magnetically along the *c* axis of the bulk hcp crystal structure. Between the Néel temperature, $T_N = 58$, and 40 K, the magnetic moments are ferromagnetically ordered within the hcp basal-plane layers and have an incommensurate sinusoidal modulation along the *c* axis. The easy axis is parallel to the *c* axis, owing to the strong crystal-field anisotropy. Upon decreasing the temperature, the propagation wave number along the *c* axis increases, and below ~30 K, a ferrimagnetic structure with a seven-layer repeat distance develops: the magnetic moments point up along the *c* axis in three layers and down in the consecutive four layers [9, 10]. As the reduction of thickness along the *c* axis could drastically influence the magnetic behavior of Tm, it is interesting to investigate the limit case of one atomic layer. Thulium grows heteroepitaxially on the W(110) surface, with the [1010] direction of the Tm layer along the [110] direction of the (110) substrate, similar to the Nishiyama-Wasserman orientation (see **Figure 1**) observed in other RE/W(110) systems [11, 12].

In nanostructured systems, there exists a strong relation between the magnetic properties of the nanostructure and its crystalline configuration and size, both being controllable by the preparation procedure. Tm on W(110) presents a large variety of morphologies depending on the coverage and thermal treatment after deposition, ranging from single atoms and clusters, to nanowires, to crystalline hexagonal monolayer islands for coverages below the monolayer and a hexagonal pyramidal Stranski-Krastanov growth for a multilayer coverage, where a

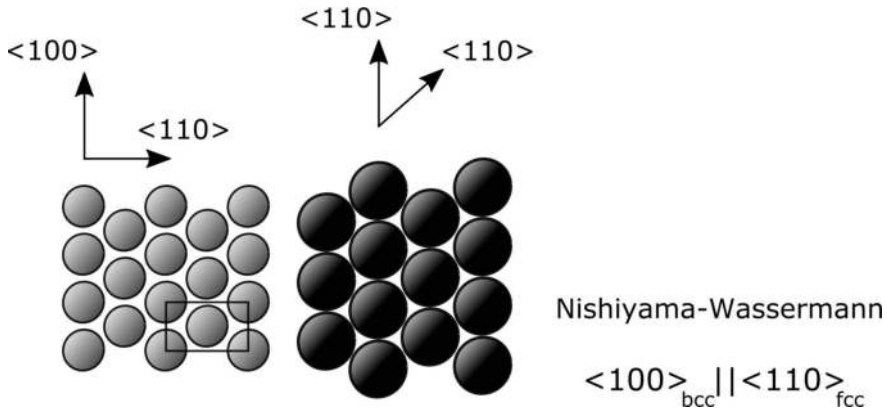

Figure 1. Nishiyama-Waserman orientation relationship for a closed-packed fcc or hcp overlayer (right) on a bcc (110) surface (left). The Miller indices of the directions in the overlayer are those appropriate for an fcc structure. Adapted from [13].

full monolayer is first formed on which subsequent pyramidal multilayer islands are able to grow. The study presented here is focused on the sub-monolayer regime and its evolution with temperature treatments. It is shown that the size of the islands can be controlled by the density of impurities on the W(110) surface, which diffuses from the bulk to the surface over time at high temperatures.

2. Experimental details

2.1. Scanning tunneling microscopy

The scanning tunneling microscope (STM) is a lensless microscope, able to bypass the diffraction limits imposed by the finite numerical aperture and wavelength, where the image is reconstructed by measuring a pointwise matrix of the interaction between the sample and a probe; the probe consists of a very sharp wire, which, when brought close enough to a metallic surface, conducts via quantum tunneling [14, 15]. By moving this probe along the surface, the variation of the tunnel current provides information of the local density of states (LDOS) at the surface of the sample, therefore making STM strictly a surface technique. Due to the exponential dependence of quantum tunneling with the width of the barrier, STM is extremely sensitive to features at the atomic scale, which goes hand in hand with the weakness of being very vulnerable to contamination at said scale. To reduce the exposure of samples to unwanted molecules, experiments are typically performed in ultra high vacuum conditions (UHV, $P \leq 10^{-10}$ mbar), maintaining vacuum unbroken along the whole experimental process, from sample preparation to STM measurements.

The STM used in this work is a SPECS Aarhus HT-STM [16], which can operate over a wide range of temperatures, 90–1300 K. A large copper block surrounds the sample acting as both temperature reservoir and damping mass to reduce vibrations. High temperatures are obtained by thermal radiation from a W filament that can be approached to the back of the sample. The STM systems are equipped with a Nanonis SPM control system for data acquisition and interfacing with the microscopes. Data treatment and analysis are performed using WSxM [17] and Gwyddion [18].

STM tips are prepared by electrochemically etching a W wire in a NaOH solution. The wire is positioned through a small flat ring where a drip of the solution is placed, forming a thin layer by surface tension, minimizing the length of the wire exposed to etching which provides for a more robust tip.

2.2. Preparation of Tm/W(110)

2.2.1. Cleaning and carbon contamination of the W(110)

The preparation of a clean W(110) surface is procedurally less complicated than other surfaces, but more demanding in the design of the heating stage and sample holder, as they involve materials such as W or Mo which are difficult to machine, but able to withstand temperatures above 2300 K.

The main contaminant in a tungsten single crystal is carbon, which is dissolved in the bulk and diffuses to the surface over time. The procedure to remove said C, described in [19], consists in annealing cycles in an oxygen-rich atmosphere ($T \sim 1500$ K, $P_{O2} \sim 5 \times 10^{-7}$ to 1×10^{-8} mbar) which causes the C adsorbates to react with the oxygen, forming CO molecules that can desorb from the surface. The second step in the procedure is to perform a short, high temperature flash of the sample ($T > 2300$ K) which removes atomic oxygen adsorbates and other remaining impurities from the sample. By performing several annealing-flash cycles, until the flashes do not produce a significant pressure spike ($P_{Flash} \leq 1 \times 10^{-10}$ mbar), a high quality clean surface is obtained. An STM image of a clean W(110) surface is shown in **Figure 2a**, with 34 adsorbates in a 40×40 nm^2 area, a ~0.3% of a monolayer. Carbon adsorbates appear as depressions on the surface, as they present a lower LDOS. To the right, **Figure 2b**, the LEED pattern corresponding to the clean surface is shown, where the rectangular lattice of the W(110) surface results in clear and well-defined spots; the [110] and [001] directions are indicated by lines.

As with any diffusion process, the rate at which C reaches the surface is strongly related to the temperature of the crystal, which during the experiments performed in this chapter is in the 700 to 1200 K range for hours at a time, strongly enhancing the C segregation. This produces a change in the quality of the surface over time, affecting the growth of Tm structures. Understanding how the surface evolves as C contamination grows is therefore important for high temperature experiments. Locally, carbon reconstruction patches will start to form where the adsorbate density is high enough; over time, the carbon reconstruction will cover the whole surface. An STM image of said reconstruction is shown in **Figure 3** accompanied by the corresponding LEED pattern showing the 15×3 relation [20].

While LEED measurements are able to distinguish between the two situations presented in **Figures 2** and **3**, quantifying the non-reconstructed adsorbate density is beyond the

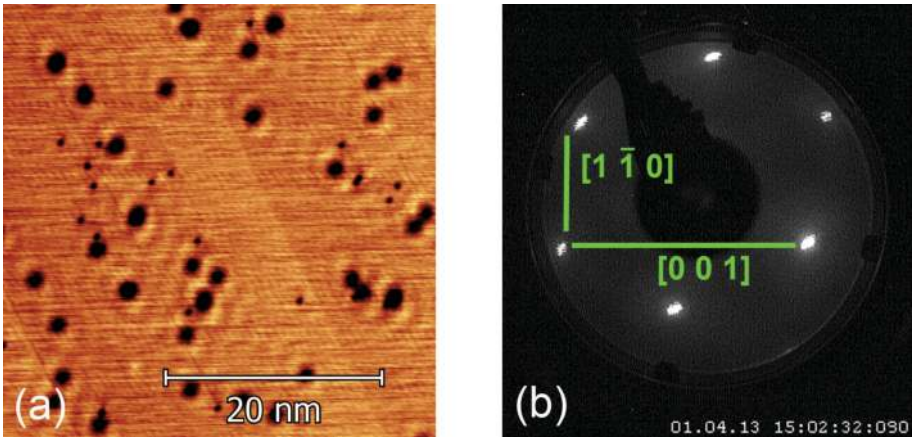

Figure 2. (a) STM image of a clean W(110) surface taken at $V_{Bias} = 100$ mV, $I_t = 1$ nA. Carbon adsorbates appear as dark spots around and serve as scatter centers for the surface state, which is clearly visible around them. (b) LEED pattern corresponding to the clean W(110) surface, with the [110] and [001] directions indicated by lines.

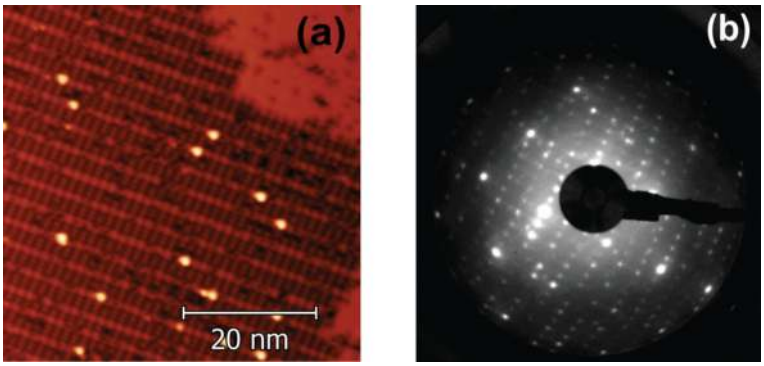

Figure 3. (a) STM image of the Carbon reconstruction on W(110) taken at V_{Bias} = 100 mV, I_t = 1 nA. (b) Corresponding LEED pattern illustrating the 15 × 3 reconstruction.

capabilities of this and other area analysis techniques (such as Auger), and STM characterization is required to ensure an adequate surface for experiments sensitive to even low densities of impurities.

2.2.2. Evaporation of Tm

Evaporation of Tm has been performed by using an electron beam evaporator. The e-beam heats a molybdenum crucible where the evaporant material is located in the form of flakes, obtaining a rate near 1 ML/min, as measured by a fluxmeter at the exit of the evaporator, where the current is proportional to the number of ions crossing the fluxmeter section per unit of time.

2.3. Tm monolayer: structural characterization

Figure 4a presents an STM image, taken at 4.2 K in a low temperature instrument, of the Tm ML along with the corresponding LEED pattern in **Figure 4d**, illustrating the situation. The STM image on the left, **Figure 4a**, shows a quasi-hexagonal symmetry on the Tm layer which should be noted is not atomic resolution, but rather a Moiré pattern caused by the overlap of the triangular Tm lattice and the rectangular W(110) surface, shown in greater detail in **Figure 4b**; the actual atomic resolution of the Tm layer can be seen in **Figure 4c**. The LEED pattern in **Figure 4d** presents the spots due the W(110) seen in **Figure 2b** and an added quasi-hexagonal structure corresponding to the Tm layer; satellite points forming an hexagon surrounding the Tm spots are due to the Moiré pattern.

The lattice parameter measured along [001] is 4.08 Å, while the two other sides of the isosceles triangle measure 3.92 Å. This means that the Tm ML displays a fairly distorted hexagonal structure, forming in fact a rhombic or isosceles triangular lattice. Thus, the lattice mismatch between Tm and W is large enough to produce in the first monolayer of thulium, an asymmetric distortion of the hcp structure that, with respect to the bulk lattice parameters, is compressed along the [110] W by 1% and expanded along [001] W by about 15%; the W lattice

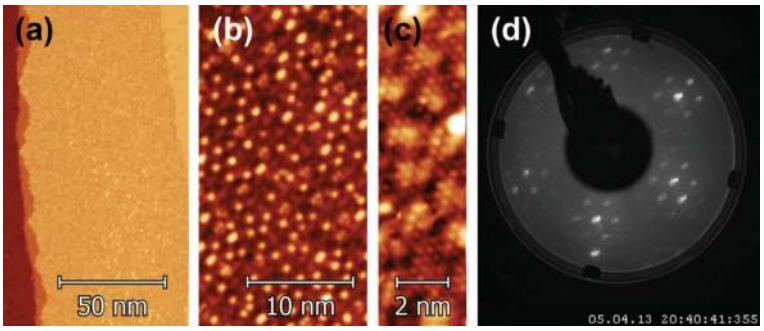

Figure 4. (a) STM image of a Tm/W(110) sample showing the Tm monolayer on W(110); the clean W surface can be seen to the sides of the Tm layer. (b) Detail of the Moiré pattern of the Tm monolayer and (c) detail of the underlying atomic resolution. (d) LEED pattern corresponding to the Tm monolayer on W(110) showing the spots corresponding to the crystalline structure surrounded by satellites corresponding to the Moiré pattern.

parameter is slightly enlarged respect to the bulk, with a_W = 3.173 Å. This results in a Tm: W coincidence match of 2:3 and 7:9 along the [110] and [001] W directions, respectively.

3. Experimental results

3.1. Low coverage: single atoms and clusters

One of the peculiarities of this system is that for low coverages, even at room temperature, single atoms and small clusters present a very low diffusion and do not aggregate into larger objects until higher temperatures, as illustrated by **Figure 5a**.

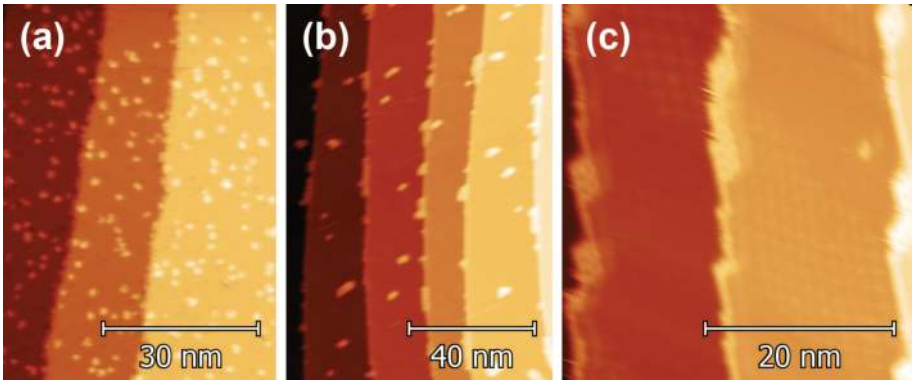

Figure 5. Tm/W(110) sample with a low Tm coverage (a) at RT, as deposited, (b) at 700 K after 4 h in the 550–700 K range, causing a high density of C adsorbates on the tungsten surface and (c) at 900 K, after 3 additional hours in the 700–900 K range, showing the surface covered in carbon reconstruction patches.

Increasing the temperature of the sample to $T = 700$ K facilitates diffusion, resulting in migration of Tm to the step edges, as well as aggregation into small islands (**Figure 5b**). It should be noted that changes in the configuration of the sample occur in a time window smaller than the thermalization time required by the system, as no strong evolution is observed at this temperature from $t_{700\,K} = 10$ to 30 min (where t_T is the time t that the sample has been at a given temperature T). Increasing the temperature above 900 K produces a notable change in the configuration, as Tm structures acquire visible hexagonal characteristics. **Figure 5c** shows the resulting sample at this temperature, where all Tm have migrated to the step edges forming a wire along the edge that expands into islands with sharp hexagonal angles.

In contrast to the previous example, a strikingly different behavior is observed for a similar starting coverage if the heating process is altered. **Figure 6a** shows the sample as deposited at room temperature, and while the coverage is roughly 1.5–2.0 times that of **Figure 5a**, it is still low enough for it to consist in small clusters as well as some atom-like objects.

In order to try and capture the diffusion process, longer time periods are spent measuring this sample at lower temperatures (600, 650, and 700 K), without observing any significant change at any given temperature, pointing to an equilibrium for the island size that is reached in the first few minutes after increasing the temperature, before the drift is low enough to allow STM measurements. Increasing the time spent at lower temperatures, however, does have a significant effect regarding the presence of C on the surface, which is much more evident in **Figure 6b** than for an equivalent temperature (730 K) reached in a shorter time, as in **Figure 5b**; the other difference between the two images is that in this case, Tm does not migrate to the step edge or form larger islands, as the diffusion process is inhibited by the presence of a large quantity of carbon adsorbates.

The difference in behavior is stronger as the temperature is increased as the large, regular islands with hexagonal characteristics, where all the Tm accumulates leaving free the majority of the tungsten surface are nowhere to be seen; instead, small irregular islands are distributed

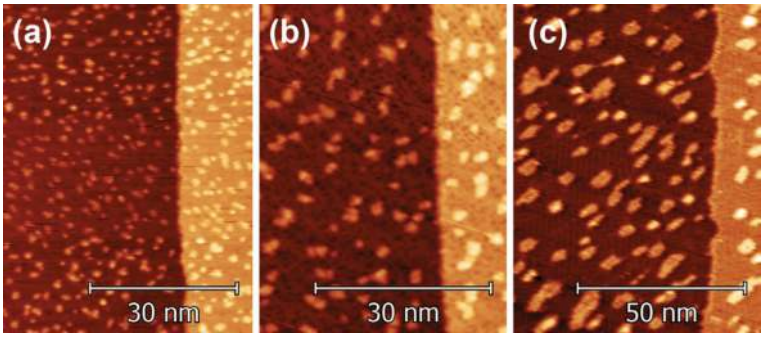

Figure 6. Tm/W(110) sample with a low Tm coverage (a) at RT, as deposited, (b) at 730 K after 4 h in the 600 to 730 K range, causing a high density of C adsorbates on the tungsten surface and (c) at 1100 K, after 3 h in the 750–1100 K range, showing the surface covered in carbon reconstruction patches.

along the surface with multiple carbon reconstruction patches covering the rest of the tungsten. **Figure 6c** shows this behavior, including double-layer islands due to the constraints imposed by the growing carbon reconstruction, even after increasing the temperature up to 1100 K.

3.2. Mid coverage: 0.5 monolayers

At higher coverages, Tm still does not tend to aggregate into a single continuous layer but rather tends to form small objects a few nanometers wide (**Figure 7a**) which, when annealed at temperatures around 600 K, evolve into small flat islands (**Figure 7b**). Following a slow heating process, as done for lower coverages, produces a similar behavior: the segregation of carbon is strongly enhanced which favors the formation of large patches of carbon reconstruction, inhibiting the diffusion of Tm and thus limiting the size of the islands; with the island size constrained by carbon, increasing the temperature up to 950 K induces a structural change where the islands become regular in shape, with hexagonal features, but without merging into large patches, but rather staying mainly as 10–15 nm wide individual islands.

It is not until the coverage is near the full monolayer that Tm does, in fact, aggregate rather than forming smaller individual objects. In this state, Tm presents a high corrugation and an irregular appearance, as seen in **Figure 8a**. Increasing the temperature to 780 K favors the mobility of Tm, allowing for the formation of a smoother but still irregular layer with a more compact structure, as shown by the fact that the tungsten surface is clearly visible in **Figure 8b** and that maintaining the sample at this temperature does not increase the proportion of visible tungsten, therefore discarding reevaporation of Tm as the cause of the observed decrease in coverage. As for the case of low coverage shown in **Figure 5**, at temperatures around 950 K, the Tm layer forms a hexagonal structure a single atomic layer in height, although in the form of large patches in this case (pictured in **Figure 8c**), as performing a faster annealing process conserves a surface clean enough for the Tm to diffuse all along the step edges, leaving the rest of the W step free of smaller Tm objects.

The evolution of the system as seen in **Figure 8** can actually be monitored by STM, as it changes in a scale of minutes. **Figure 9** shows the same area of the course of 30 min at $T = 780$ K, showing a dynamic behavior. The evolution pictured occurs 40 min after setting the temperature

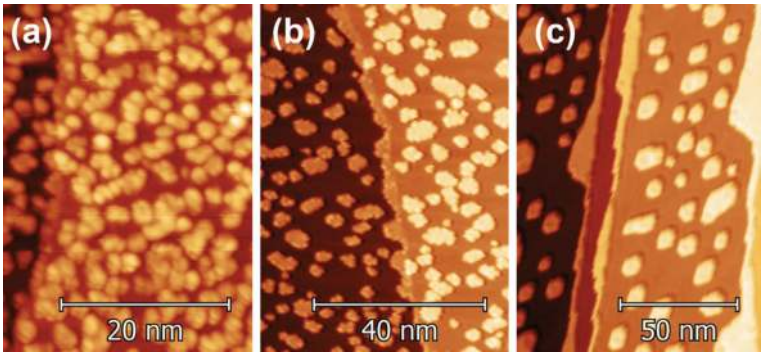

Figure 7. Tm/W(110) sample with coverage near 0.5 ML (a) at RT, as deposited, in the form of irregular islands (b) at 750 K showing flatter, but still irregular islands and (c) at 950 K, where the diffusion is limited by the presence of C reconstruction patches and Tm takes the form small islands with hexagonal features.

http://dx.doi.org/10.5772/intechopen.70218

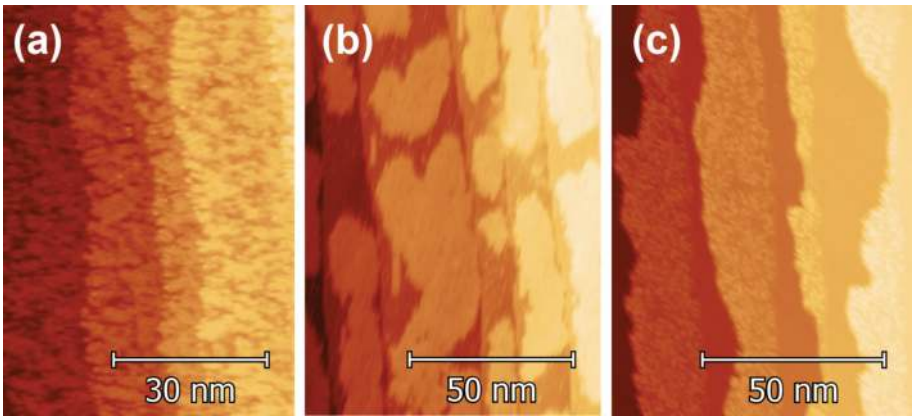

Figure 8. Tm/W(110) sample with a coverage around 0.5 ML coverage (a) as deposited at RT (b) at 750 K and (c) at 950 K. Islands change from irregular and rough in (b) to the crystalline with a Moiré pattern (c) for higher temperatures.

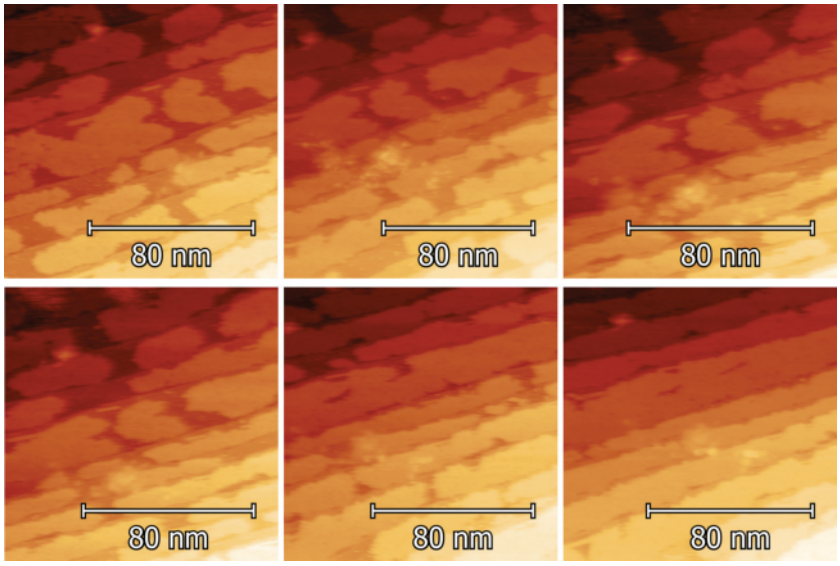

Figure 9. From left to right, top to bottom: Evolution over 30 min of the sample at 750 K. Thulium islands expand, covering the whole surface.

set point; some self-assembled nanowires can be seen in the first images, although the overwhelming majority of Tm is forming irregular-shaped islands. Over time, the islands expand, approaching the full monolayer and covering the wire structures. As no new material is added during this time, the increase in surface covered by the Tm islands is due to the system evolving to a new, less compact configuration. At higher temperatures, this is then followed by a structural change into a more compact hexagonal lattice, as seen from **Figure 8b** and **c**.

3.3. High coverage: above 1 monolayer

For higher initial coverages, above the monolayer, the Stranski-Krastanov growth mode is evident, with Tm forming multiple-layer high hexagonal pyramids in **Figure 10a**. Annealing this sample illustrates the origin of this growth mode: the W-Tm interface is energetically more favorable than the Tm-Tm interface; therefore, completion of the initial wetting layer takes priority over subsequent layers, as illustrated by the fact that the said higher Tm layers are reevaporated at lower temperatures than the wetting layer. Thus, annealing at high temperature, a multilayer sample, such as **Figure 10a**, leads to a similar result as for submonolayer samples, with the already discussed heteroepitaxial monolayer with a Moiré pattern, pictured in **Figure 10b**.

At high temperatures, carbon segregation to the surface is fast enough to observe its effect over consecutive scans. **Figure 11** shows the same area of the Tm monolayer at 1000 K over the course of 5 min. The small dark patch in **Figure 11a** is an area with carbon reconstruction which grows over time, while other small patch appears (**Figure 11b**), eventually merging with each other, forming a larger area of carbon reconstruction along the step edge. The growth of the carbon reconstruction patches displaces Tm from the layer, rather than growing below it, as it can be seen in **Figure 11b** and **c**: small areas on the Tm layer with a greyer color appear to have carbon beneath, while a darker area, similar in hue to the reconstruction along the step edge, seems to have displaced the Tm layer.

This effect is also seen on other samples, as shown in **Figure 12**, while the time evolution is not captured, it can be seen that Tm is displaced by the carbon reconstruction onto the second layer in **Figure 12a**, and 30 min later in **Figure 12b**, the Tm layer is flat once again, with Tm organized along to the step edge and carbon adsorbates and reconstruction patches on the outer side of the step. As the coverage is lower than the initial, it suggests a reevaporation at this temperature of the material that moves onto the second layer.

In this case, the carbon reconstruction patches within the layer have grown to the point where it is favorable for Tm to move to the second layer. Over time, this Tm is reevaporated reducing the total coverage, while the remaining material reorganizes forming a continuous layer with the carbon reconstruction patches along the step edges.

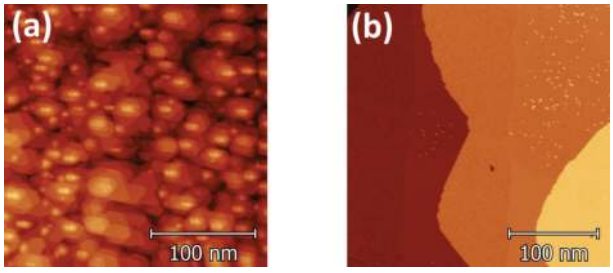

Figure 10. (a) Multilayer Thulium sample as deposited at room temperature showing hexagonal pyramidal islands. (b) After annealing at 1100 K, leaving only monolayer Tm islands on the W(110) surface; carbon reconstruction patches can also be seen.

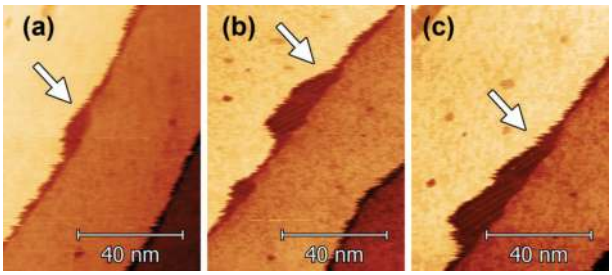

Figure 11. Evolution over 5 min of the sample at 1000 K, showing the growth of a carbon reconstruction patch, displacing the Tm layer: (a) At eh beginning, (b) the time between and (c) at the end of the sequence.

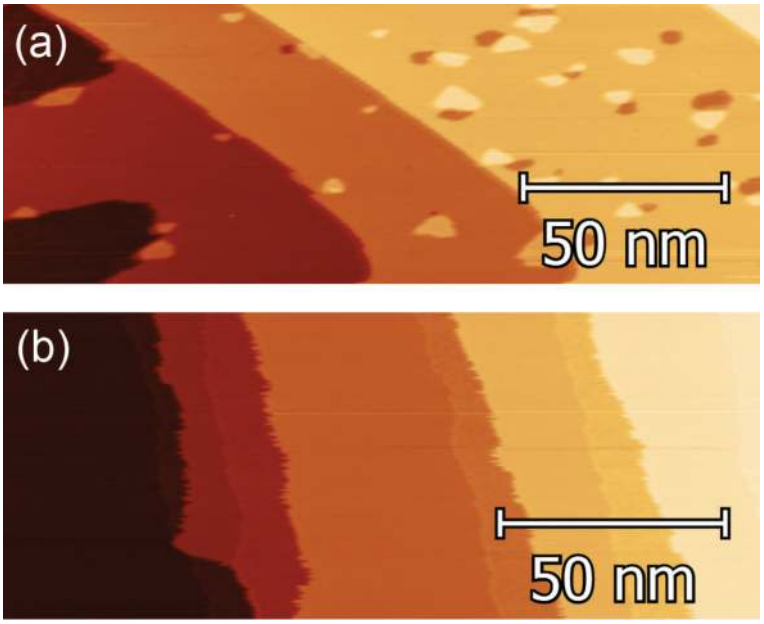

Figure 12. (a) Tm being displaced by carbon reconstruction patches at 1050 K. (b) The same sample 30 min later while keeping the temperature at 1050 K, showing that Tm has compensated for the displaced material by migrating to the step edge.

4. Analysis

4.1. Size distribution of Tm islands

To study the effect of carbon adsorbates on the diffusion of Tm on the W(110) surface and thus on the resulting island size, it is interesting to first introduce the basic ideas involved in

the description of nucleation on ideal surfaces, omitting the effect of impurities, anisotropies, steps, and other deviations from a perfect surface.

Once an atom or molecule is absorbed onto a surface, it can be reevaporated or diffused along the surface. Adatoms diffusing on the surface can encounter each other leading to the formation of dimers, clusters, and larger two-dimensional islands. These islands, as a whole, are stable and do not diffuse further; their shape and size, however, can change by dissociation and diffusion of the adatoms on the edges.

Island nucleation and growth (precoalescence stage) continues until islands grow to the point of merging with each other. At this point, continued growth of the layer consists in the filling of the remaining holes (post-coalescence stage). Thus, at constant temperature, the number of islands increases over time until coalescence between them begins, reducing the total number of individual islands. For the case of three dimensional islands, if no additional material is deposited on top of the island, but rather there is a transference between layers, overcoming the Ehrlich-Schwoebel energy barrier associated with the interlayer jumping is required.

The behavior of single-component metallic systems is well understood, based on scaling properties of measured island densities and shapes as a function or temperature and covering. Several reviews present a thorough presentation of the state of the art [21, 22]. Usually, the diffusion process is presented in the context of a clean surface: only the adatoms and the surface are considered to obtain the relevant parameters [23]. In some cases of practical interest, the diffusion happens on surfaces partly covered by other impurities, and the diffusion is modified with respect to that observed in a clean surface, e.g., adsorbed hydrogen atoms enhances the self-diffusion of Pt by two orders of magnitude [24].

4.1.1. Island density

Two factors influence the nucleation and growth of islands: Deposition of atoms onto the surface with a flux F and thermally activated diffusion of adatoms along the surface with a diffusion coefficient D:

$$D = D_0 \exp(-U/k_B T) \tag{1}$$

where U is the diffusion barrier and k_B the Boltzmann constant. For atomic systems, $D_0 = \nu a^2$, where ν is an attempt frequency, and a is the lattice constant of the substrate. Thus, with the definitions of F and D, the mean time for a unit cell to be hit by an atom is $1/Fa^2$, and the mean time after which the atom leaves the cell by diffusion is a^2/D. Some conclusions can be obtained observing Eq. (1): adatom diffusion is thermally activated, thus increasing temperature produces an increment of D, and adatoms can diffuse over longer distances. As a result, the density N of stable islands becomes smaller with increasing T, and the number of atoms forming the island increases.

In order to describe and quantify the structures observed by STM or AFM as function of coverage Θ or temperature, a complete set of equations has been obtained in the literature [21]. A fundamental concept is the critical island size or critical nucleus i. This variable denotes the critical cluster size, which becomes stable on adding an atom. Clusters with $i+1$ atoms are more likely to grow than to dissociate. i depends on the substrate temperature, increasing

when T increases, and other factors as the crystal symmetry of the substrate and the structure of a film, either amorphous or crystalline.

4.1.2. Mean field calculation

The mean-field nucleation theory has been used to obtain a simple expression for the concentration n_x of 2-D islands of size i for the case of complete condensation [21, 22, 25]:

$$n_x \propto \left(\frac{D}{F}\right)^{-\chi} \exp\left[\frac{E_i}{(i+2)\,k_B T}\right] \tag{2}$$

where $\chi = i/(i+2)$, and E_i is its bonding energy. A stable cluster means that it grows more rapidly than it decays, for instance by a dissociation process, during the course of deposition.

4.2. Influence of carbon adsorbates in island size

While the discussion above pertains to the case of clusters with a small number of atoms, the dependence of the equilibrium island size with temperature is a general conclusion. **Figure 13** shows the island size evolution with temperature of a sample, where little carbon has segregated over the whole sequence, leading to a final island size that is actually limited by the step size, as seen in the lower section of **Figure 13**, illustrating the sample at different stages.

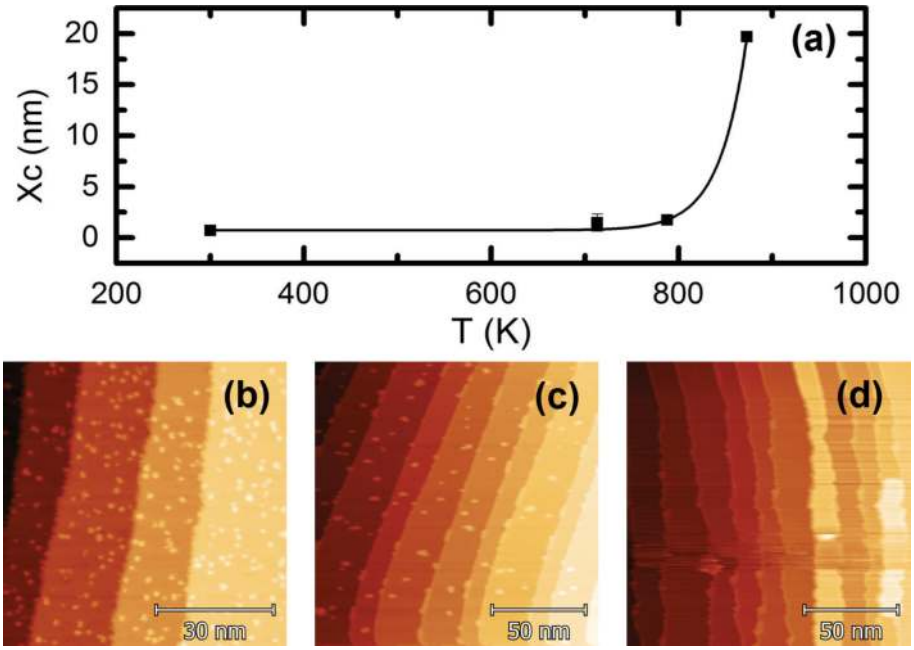

Figure 13. (a) Island size evolution with temperature. Below, from left to right, the evolution of the island size on the same sample at (b) room temperature, (c) 730 K and (d) 950 K. Note that the island size at high T is limited by the step size.

This is in stark contrast with the behavior described for samples, where the annealing process is performed over a longer time, allowing for a greater density of carbon adsorbates on the surface, as seen previously in **Figures 6** and **7**. Plotting the island size as a function of temperature for several samples illustrates how different the behavior is between a clean surface and one saturated with the 15 × 3 carbon reconstruction.

It is not trivial to quantify the number of impurities, especially with experiments at high temperature where resolution might be compromised to avoid risking tip crash, further complicated by drift issues. **Figure 14** shows the island size evolution for several sets of samples, divided roughly in three categories depending on the carbon density on the surface: Low Carbon (blue hues in the graph), where the sample remains reasonably clean after the annealing process and island size is limited mainly by the size of the steps and the amount of Tm available; Mid Carbon, where carbon reconstruction patches and a high density of carbon adsorbates strongly limit the mean island size; High Carbon, with carbon reconstruction patches covering the whole surface.

A careful control over the carbon density on the W(110) surface can thus provide a reliable method for obtaining self-assembled islands with a definite size, ranging from being limited by the atomic step size to islands under 5 nm in diameter.

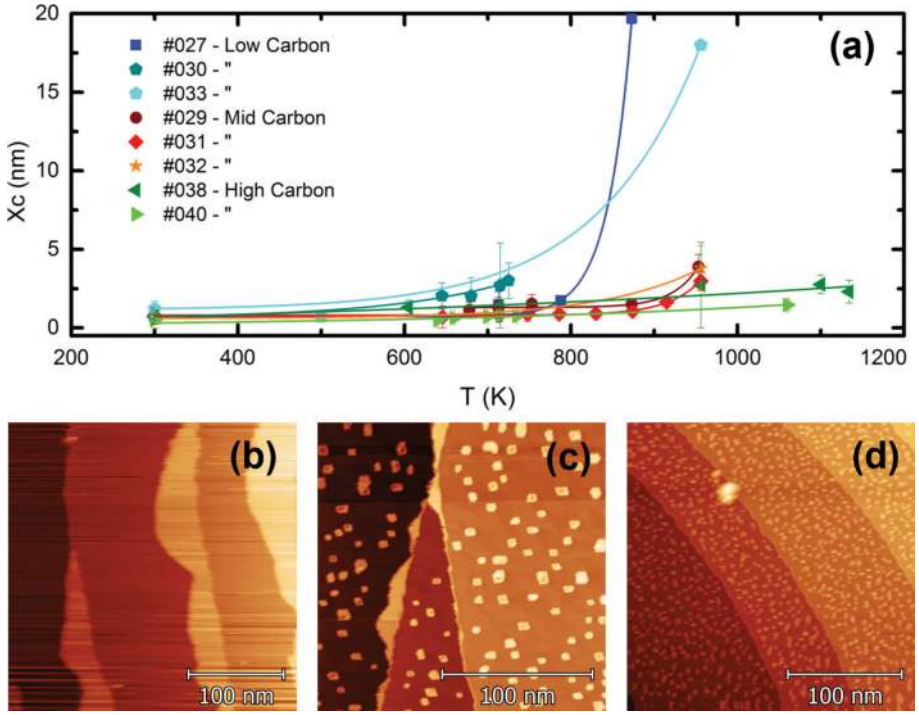

Figure 14. (a) Island size evolution with temperature for a set of samples. Below, representative final states for different samples, corresponding to the curves marked as (b) sample 030 at a final temperature of 950 K, with low carbon presence resulting in large islands; (c) sample 031 at 950 K, with a strong presence of carbon reconstruction, but segregated after the islands already increased in size; and (d) sample 040 at 1050 K, where very small regular islands can be observed all over the surface, due to the inhibited diffusion due to the high density of carbon on the surface.

5. Conclusion

In this chapter, the preparation of single atomic layer Tm films on a W(110) substrate is explored. Sub-monoloyer Tm deposits can present a varied morphology depending on initial coverage, substrate temperature and adsorbate density. The key to achieving high-quality pseudomorphic Tm films resides in an annealing process after evaporation, which motivates the study presented here, where STM experiments are performed at high temperature to observe in situ the evolution of the Tm film. Measurements over time evidence the diffusion of carbon adsorbates from the bulk of the W crystal onto the surface. The effect of carbon impurity density on the diffusion process of Tm atoms is studied by observing the evolution of multiple samples at different initial coverages following different thermal processes, with longer times leading to a higher adsorbate density. It is observed that the presence of carbon strongly limits the diffusion of Tm, thus leading to the formation of pseudomorphic nanometric islands instead of the full monolayer. The ultimate result of the procedure described in this chapter indicates that with careful control of the impurity density, structures with mean Tm island size down to 5 nm in diameter can be obtained, an interesting achievement considering that the magnetic anisotropy of Tm foresees perpendicular magnetization in these islands. This work highlights the role of surface adsorbates on the diffusion process of single atoms, and how it governs the nucleation of islands; experimental evidence is presented of control over the mean island size by means of inducing a change in the diffusion parameters on the surface in a controlled fashion by using impurities existing in the substrate, a procedure that could be extrapolated to other magnetic materials to create self-ensembled nanosystems.

Acknowledgements

This work was supported by the Spanish MICINN (Grants MAT2015-66726-R and MAT2013-46593-C6-3-P), Gobierno de Aragón (Grant E81), and Fondo Social Europeo. We thank Dr. José Luis Diez-Ferrer for providing the images of **Figure 3**.

Author details

David Coffey[1,2,3], José I. Arnaudas[2,3], David Serrate[2,3] and Miguel Ciria[1,3]*

*Address all correspondence to: miguel.ciria@csic.es

1 Instituto de Ciencia de Materiales de Aragón, Consejo Superior de Investigaciones Científicas, Zaragoza, Spain

2 Laboratorio de Microscopías Avanzadas, Fundación Instituto de Nanociencia de Aragón, Universidad de Zaragoza, Zaragoza, Spain

3 Departamento de Física de la Materia Condensada, Universidad de Zaragoza, Zaragoza, Spain

References

[1] Kwo J, Gyorgy EM, McWhan DB, et al. Magnetic and structural properties of single-crystal rare-earth Gd-Y superlattices. Physical Review Letters. 1985;**55**:1402-1405

[2] Weller D, Alvarado SF, Gudat W, et al. Observation of surface-enhanced magnetic order and magnetic surface reconstruction on Gd(0001). Physical Review Letters. 1985; **54**:1555-1558

[3] Kwo J, Hong M, Nakahara S. Growth of rare-earth single crystals by molecular beam epitaxy: The epitaxial relationship between hcp rare earth and bcc niobium. Applied Physics Letters. 1986;**49**:319-321

[4] Majkrzak CF, Cable JW, Kwo J, et al. Observation of a magnetic antiphase domain structure with long-range order in a synthetic Gd-Y superlattice. Physical Review Letters. 1986;**56**:2700-2703

[5] Salamon MB, Sinha S, Rhyne JJ, et al. Long-range incommensurate magnetic order in a Dy-Y multilayer. Physical Review Letters. 1986;**56**:259-262

[6] Kolaczkiewicz J, Bauer E. The adsorption of Eu, Gd and Tb on the W(110) surface. Surface Science. 1986;**175**:487-507

[7] Nicklin CL, Binns C, Norris C, et al. Valence state of low-dimensional thulium structures grown on molybdenum (110). Surface Science. 1994;**307-309**:858-862

[8] Bodenbach M, Höhr A, Laubschat C, et al. Surface electronic structure of Tm(0001) and Yb(111). Physical Review B. 1994;**50**:14446-14451

[9] Koehler WC, Cable JW, Wollan EO, et al. Magnetic structures of thulium. Physical Review. 1962;**126**:1672-1678

[10] Brun TO, Sinha SK, Wakabayashi N, et al. Temperature dependence of the periodicity of the magnetic structure of thulium metal. Physical Review B. 1970;**1**:1251-1253

[11] Li H, Tian D, Quinn J, et al. Structural and electronic properties of ultrathin films of Gd, Tb, Dy, Ho, and Er. Physical Review B. 1992;**45**:3853-3856

[12] Tober ED, Ynzunza RX, Westphal C, et al. Relationship between morphology and magnetic behavior for Gd thin films on W(110). Physical Review B. 1996;**53**:5444-5448

[13] Barret S, Dhesi S. The Structure of Rare-Earth Metal Surfaces. London: Imperial C; 2001

[14] Binnig G, Rohrer H, Gerber C, et al. Surface studies by scanning tunneling microscopy. Physical Review Letters. 1982;**49**:57-61

[15] Binnig G, Rohrer H. Scanning tunneling microscopy. Helvetica Physica Acta. 1982;**55**:726

[16] Petersen L, Schunack M, Schaefer B, et al. A fast-scanning, low- and variable-temperature scanning tunneling microscope. Review of Scientific Instruments. 2001;**72**:1438

[17] Horcas I, Fernández R, Gómez-Rodríguez JM, et al. WSXM: A software for scanning probe microscopy and a tool for nanotechnology. Review of Scientific Instruments. 2007;**78**:13705

[18] Nečas D, Klapetek P. Gwyddion: An open-source software for SPM data analysis. Central European Journal of Physics. 2012;**10**:181

[19] Bode M, Krause S, Berbil-Bautista L, et al. On the preparation and electronic properties of clean W(110) surfaces. Surface Science. 2007;**601**:3308

[20] Bode M, Pascal R, Wiesendanger R. STM study of carbon-induced reconstructions on W(110): Strong evidence for a surface lattice deformation. Surface Science. 1995;**344**:185-191

[21] Brune H. Microscopic view of epitaxial metal growth: Nucleation and aggregation. Surface Science Reports. 1998;**31**:121-229

[22] Einax M, Dieterich W, Maass P. *Colloquium* : Cluster growth on surfaces: Densities, size distributions, and morphologies. Reviews of Modern Physics. 2013;**85**:921-939

[23] Brune H, Bales GS, Jacobsen J, et al. Measuring surface diffusion from nucleation island densities. Physical Review B. 1999;**60**:5991-6006

[24] Horch S, Lorensen HT. Enhancement of surface self-diffusion of platinum atoms by adsorbed hydrogen. Nature. 1999;**398**:134

[25] Venables JA. Nucleation calculations in a pair-binding model. Physical Review B. 1987;**36**:4153-4162